

Superconductivity from Doping Symmetric Mass Generation Insulators: Application to $\text{La}_3\text{Ni}_2\text{O}_7$ under Pressure

Da-Chuan Lu,¹ Miao Li,² Zhao-Yi Zeng,³ Wanda Hou,¹ Juven Wang,⁴ Fan Yang,⁵ and Yi-Zhuang You¹

¹*Department of Physics, University of California, San Diego, CA 92093, USA*

²*School of Physics, Zhejiang University, Hangzhou 310027, China*

³*School of Physics, Fudan University, Shanghai 200438, China*

⁴*Center of Mathematical Sciences and Applications,*

Harvard University, Cambridge, Massachusetts 02138, USA

⁵*School of Physics, Beijing Institute of Technology, Beijing 100081, China*

We investigate the bilayer nickelate as a platform to realize the symmetric mass generation (SMG) insulator, a featureless Mott insulator that arises due to the Lieb-Schultz-Mattis (LSM) anomaly cancellation in bilayer spin-1/2 lattice systems. Through a single-orbital bilayer square lattice model involving intralayer hopping t and interlayer superexchange interaction J , we demonstrate the emergence of high-temperature superconductivity (SC) upon doping the SMG insulator. The SC phase features s -wave interlayer spin-singlet pairing and exhibits a crossover between the Bardeen-Cooper-Schrieffer (BCS) and Bose-Einstein condensation (BEC) limits by tuning the J/t ratio. We estimate the SC transition temperature T_c from both the weak and strong coupling limits at the mean-field level. Our findings offer insights into the experimentally observed decrease in T_c with pressure and the strange metal behavior above T_c . Additionally, we propose that both Ni $3d_{z^2}$ and $3d_{x^2-y^2}$ orbitals can exhibit superconductivity in $\text{La}_3\text{Ni}_2\text{O}_7$ under pressure, but their T_c should vary in opposite ways under doping. This characteristic difference suggests a potential experimental pathway to identify which electronic orbital plays the principal role in the formation of superconductivity in this system.

I. INTRODUCTION

The recent experimental discovery [1–4] of high-temperature superconductivity (SC) in single crystals of $\text{La}_3\text{Ni}_2\text{O}_7$ under high pressure has uncovered an exciting platform for investigating and testing unconventional SC mechanisms [5, 6] in condensed matter physics. This nickelate compound, when driven into a pressure-induced orthorhombic phase with $Fmmm$ spacegroup symmetry, manifests superconductivity, with an observed maximum transition temperature (T_c) of 80K within a pressure range of 14.0 to 43.5GPa [1].

Density-functional-theory (DFT) based first-principles calculations indicate that the low-energy behavior in $\text{La}_3\text{Ni}_2\text{O}_7$ is governed by two e_g orbitals of Ni: $3d_{x^2-y^2}$ and $3d_{z^2}$ [1, 7–11]. Within a unit cell, the two d_{z^2} orbitals in distinct layers can couple through hybridization with the apical oxygen’s p -orbital in the charge-reservoir layer. When subjected to pressure, the Ni-O-Ni bonding angle shifts from 168° to 180° , remarkably enhancing the interlayer coupling. The emergence of SC solely under pressure implies that this interlayer coupling is likely pivotal to the pairing mechanism. Additionally, the robust electron-electron interaction in the Ni- $3d$ orbitals could drive the SC, in line with recent experimental findings that $\text{La}_3\text{Ni}_2\text{O}_7$ is in proximity to a Mott phase and exhibits non-Fermi-liquid behaviors [2, 4].

Two remarkable features of the $\text{La}_3\text{Ni}_2\text{O}_7$ superconductor stand out: First, its T_c intriguingly decreases with increasing pressure, a behavior challenging the standard phonon or magnon-mediated pairing mechanism, since higher pressures typically imply stronger lattice vibrations and magnetism energy scales, which would other-

wise lead to higher T_c . Secondly, above T_c , the compound displays a “strange metal” behavior, characterized by a linear temperature-dependent resistivity up to 300K [1, 2, 4], which suggests the presence of strong quantum fluctuations or proximity to quantum critical points.

The theoretical framework to comprehensively explain these intriguing features is still under development. On the weak-coupling side, studies employing the functional renormalization group [12, 13], fluctuation-exchange approach [11], and random-phase approximation [14–17] have been conducted. The majority of these point to the s^\pm -wave pairing [11–16], driven by spin fluctuations. In these models, the nesting between the emergent γ -pocket under pressure and the previously existing β -pocket plays a crucial role in the s^\pm -wave pairing. On the strong-coupling side, various models have been established, involving different types of superexchange interactions [11–13, 18–26]. Although most emphasize the significance of the interlayer exchange between the two d_{z^2} orbitals within a unit cell, differing opinions exist on the dominant orbital contributing to SC, which can be either d_{z^2} [11, 18, 24] or $d_{x^2-y^2}$ [21–23, 26]. Currently, a consensus has not been reached regarding which orbital contributes more significantly to SC, and a unified physical understanding remains elusive.

Our study aims to establish a simple theoretical model that encapsulates the main features of the pressurized nickelate high-temperature superconductor. Specifically, we propose to understand the high- T_c superconductivity in $\text{La}_3\text{Ni}_2\text{O}_7$ from the perspective of doped Symmetric Mass Generation (SMG) [27–34] insulators. One critical distinction between nickelate and cuprate superconductors lies in their lattice structures: nickelates have a

bilayer lattice structure with a strong interlayer superexchange, while cuprates typically consist of decoupled single layers. This difference results in fundamentally contrasting Mott insulating states when these systems are at half-filling, particularly in regard to the Lieb-Schultz-Mattis (LSM) [35–39] anomaly.

In the cuprates, the Mott insulator is constrained by the LSM theorem to possess a non-trivial ground state, meaning that the cuprate Mott state must either spontaneously break the symmetry or develop a topological order [40, 41]. Conversely, nickelates are not restricted by the LSM theorem as the LSM anomaly (at half filling) falls under the \mathbb{Z}_2 classification. Thus, the bilayer system is anomaly-free and can form a trivial Mott insulator under interaction, which is referred to as an SMG insulator. Doping an SMG insulator also leads to superconductivity, but the underlying mechanisms differ significantly from those of the traditional doped Mott insulator.

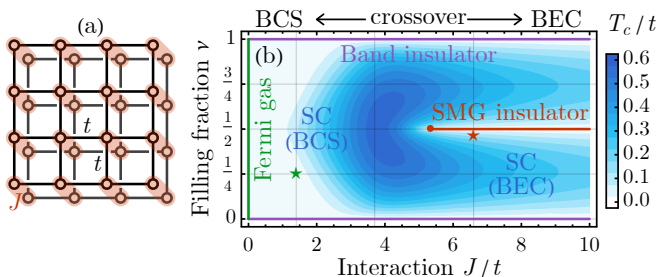


FIG. 1. (a) The proposed bilayer square lattice model, featuring intralayer hopping t and interlayer Heisenberg interaction J . (b) Mean-field phase diagram, dominated by a single SC phase (blue) with s -wave interlayer spin-singlet pairing, alongside Fermi gas (green), band insulator (purple), and SMG insulator (red) lines. The shading in blue illustrates the SC transition temperature T_c , which crosses over between BCS and BEC regimes depending on J/t . Red and green stars highlight parameters relevant to the Ni- $3d_{z^2}$ and $3d_{x^2-y^2}$ electrons in $\text{La}_3\text{Ni}_2\text{O}_7$, respectively.

More specifically, we propose a bilayer square lattice model Fig. 1(a) with interlayer antiferromagnetic Heisenberg interaction to demonstrate the key physics of an SMG insulator. A mean-field phase diagram is shown in Fig. 1(b). The emergent SC in the doped SMG insulator can be interpreted within the theoretical framework of the BCS-BEC crossover [42, 43]. The observed decrease in T_c with increasing pressure indicates that the system resides on the Bose-Einstein condensate (BEC) side. Pictorially, the SMG insulator can be viewed as a Mott insulating state [44–46] of interlayer spin-singlet Cooper pairs [47, 48]. The pairing energy for these Cooper pairs stems from the interlayer spin interaction. Upon doping, these preformed Cooper pairs become mobile on the lattice, developing a BEC state at low temperatures, which can be interpreted as an s -wave interlayer spin-singlet SC state from the electron’s perspective. The BEC-side SC phase exhibits three characteristics:

- (i) The critical temperature T_c decreases with increasing interlayer Heisenberg interaction, which can typically be realized by increasing the pressure exerted on the material.
- (ii) Above T_c , the system enters a pseudo-gap (PG) phase, where phase-incoherent preformed Cooper pairs fluctuate in the background. These low-energy fluctuations scatter the itinerant electrons, leading to a strange metal behavior in the system.
- (iii) The optimal doping (for maximal T_c) occurs near 50% (i.e., $1/4$ filling of electrons) because the interlayer Cooper pairs have the highest mobility at this level, and can most easily establish the phase coherence that is needed for SC.

Combining with the theoretical analysis of the bilayer square lattice model, evidence suggests that both d_{z^2} and $d_{x^2-y^2}$ orbitals can contribute to superconductivity in $\text{La}_3\text{Ni}_2\text{O}_7$. However, distinguishing between these two possibilities requires a closer examination of how the critical temperature T_c depends on doping. If superconductivity is primarily governed by the BCS mechanism acting on $d_{x^2-y^2}$ electrons, then T_c will rise with *electron* doping. Conversely, if the BEC mechanism governing d_{z^2} electrons predominates, T_c will increase with *hole* doping. These contrasting behaviors in the doping dependence of T_c offer potential experimental pathways for determining the electronic orbital origin of superconductivity in this system.

The remainder of this paper is structured as follows. We begin with a brief review of the local electronic structure of $\text{La}_3\text{Ni}_2\text{O}_7$ in Sec. II A, upon which we construct a minimal bilayer square lattice model, as detailed in Sec. II B. The symmetry and anomaly analysis, along with an introduction to the SMG insulator, are discussed in Sec. III A. The emergence of SC from doping the SMG insulator is then examined from both weak-coupling (Sec. III B) and strong-coupling (Sec. III C) perspectives, with a unification of these results in Sec. III D. We reflect on the implications of our findings for nickelate superconductors in Sec. IV A and briefly explore other strong correlation effects as a supplement to our model in Sec. IV B. The paper concludes with a summary in Sec. V.

II. MODELING

A. Local Electronic Structure

The bulk single crystal $\text{La}_3\text{Ni}_2\text{O}_7$ is constructed from an infinite stack of NiO_2 bilayers, see Fig. 2(a). The nickel elements in the compound have a valence of $\text{Ni}^{2.5+}$, corresponding to a $3d^{7.5}$ electronic state. Within this state, 6 electrons fully occupy the t_{2g} orbitals (d_{xz} , d_{yz} , d_{xy}), while the remaining 1.5 electrons populate the e_g orbitals (d_{z^2} , $d_{x^2-y^2}$). On average, about one electron is

on the d_{z^2} orbital (half filling the d_{z^2} band, filling fraction $\nu = 1/2$), and on-average 0.5 electron is on the $d_{x^2-y^2}$ orbital (quarter filling the $d_{x^2-y^2}$ band, filling fraction $\nu = 1/4$). However, these filling fractions are not fixed, as charge transfer between the two e_g orbitals might occur under pressure. Density functional theory (DFT) calculations [7, 8] indicate that the electronic structure near the Fermi surface is primarily derived from the d_{z^2} and $d_{x^2-y^2}$ orbitals of nickel and the $p_{x/y/z}$ orbitals of oxygen. The dominant hopping is between the d_{z^2} orbitals across the vertical Ni-O-Ni bond, denoted as $t_{\perp} \approx 0.64$ eV in Fig. 2(b), and among the $d_{x^2-y^2}$ orbitals across in-plane Ni-O-Ni bonds, denoted as $t \approx 0.48$ eV in Fig. 2(c). The other hopping processes are found to be parametrically small [7, 8].

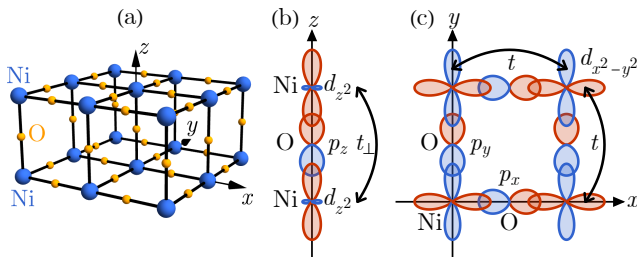


FIG. 2. (a) Lattice structure of the NiO₂ bilayer. (b) Interlayer hopping t_{\perp} of d_{z^2} electron through the Ni-O-Ni bond. (c) Intralayer hopping t of $d_{x^2-y^2}$ electron through the Ni-O-Ni bond.

Whether the SC arises from the d_{z^2} electron or the $d_{x^2-y^2}$ electron remains a subject of debate. We attempt to identify the unique features of these two possibilities through a unified toy model and compare them with experimental observations.

Firstly, considering the electron interaction effect, the most prominent local physics within each unit cell is the interlayer antiferromagnetic Heisenberg interaction between d_{z^2} electrons. This arises from the superexchange mechanism across the vertical Ni-O-Ni bond, and the coupling strength is estimated to be of the order $J = 4t_{\perp}^2/U \simeq 0.66$ eV, assuming a Hubbard interaction around $U \simeq 2.5$ eV. Given that the half-filled d_{z^2} orbital corresponds to two electrons per unit cell, the electrons naturally pair up into interlayer spin-singlets in each unit cell, forming a featureless Mott insulator [49] without symmetry-breaking or topological orders. This insulating state is also referred to as the SMG insulator, defined as a featureless Mott insulator without LSM anomaly (or Fermi surface anomaly), which is only achievable when each unit cell hosts linear representations of internal symmetries (or integer filling of electrons), as is the case here.

Next, given the ferromagnetic Hund's rule interaction between the $d_{x^2-y^2}$ and d_{z^2} electrons within each Ni atom, an interlayer antiferromagnetic Heisenberg interaction between the $d_{x^2-y^2}$ electrons can be induced [21, 22], on the d_{z^2} orbital-selective interlayer spin-singlet back-

ground [8]. The coupling strength J is roughly the same as that for the d_{z^2} electrons [21, 22]. However, since the $d_{x^2-y^2}$ electron has a quarter filling only, and its intralayer hopping $t \simeq 0.48$ eV is on a scale close to $J \simeq 0.66$ eV, it has more freedom to hop around the lattice and is expected to be closer to the Fermi liquid state, away from the SMG insulating limit.

Overall, the d_{z^2} electrons are more localized in the unit cell, exhibiting strong coupling physics; while the $d_{x^2-y^2}$ electrons are more itinerant on the square lattice, demonstrating weak coupling physics. We conclude that, for both d_{z^2} and $d_{x^2-y^2}$ electrons, the competition between interlayer spin-spin interaction J and intralayer hopping t is key to understanding their low-energy physics.

B. Minimal Lattice Model

Based on this insight, we postulate to ignore other interactions and band structure details, and first focus on the following minimal model on the bilayer square lattice, as depicted in Fig. 1(a),

$$H = t \sum_{\langle ij \rangle, l} (c_{i\uparrow}^{\dagger} c_{j\downarrow} + \text{h.c.}) - \mu \sum_{il} c_{i\uparrow}^{\dagger} c_{i\downarrow} + J \sum_i \mathbf{S}_{i1} \cdot \mathbf{S}_{i2}, \quad (1)$$

where $c_{il} = (c_{i\uparrow}, c_{i\downarrow})^{\top}$ denotes a spin-1/2 electron annihilation operator on the unit cell i and the layer $l = 1, 2$, and $\mathbf{S}_{il} := \frac{1}{2} c_{i\uparrow}^{\dagger} \boldsymbol{\sigma} c_{i\downarrow}$ is the electron spin operator. We ignore the on-site Hubbard interaction for now and will comment on its physical effect later. We do not impose any on-site single-occupancy constraint, such that the electron filling can be adjusted from $\nu = 0$ (empty) all the way to $\nu = 1$ (four electrons per unit cell). The model may describe either d_{z^2} or $d_{x^2-y^2}$ electrons depending on the parameter choice. Here, t represents the intralayer (in-plane) hopping, J represents the interlayer spin interaction, and the chemical potential μ tunes the electron filling. Similar models have previously appeared in the literature [34, 50–56], and recently proposed to describe the La₃Ni₂O₇ superconductor [18, 19, 21–24]. Recent research [34] has revealed that the bilayer square lattice model features a Fermi surface SMG [32] phase at half-filling.

The model respects the bilayer square lattice space group symmetry, including the 2D lattice translation symmetry $\mathbb{Z} \times \mathbb{Z}$. It also has an internal symmetry of

$$G_{\text{general}} = \text{SU}(2) \times_{\mathbb{Z}_2^{\text{F}}} (\text{U}(1)_1 \times \text{U}(1)_2), \quad (2)$$

which includes the spin SU(2) symmetry (generated by $\mathbf{S} = \sum_{il} \mathbf{S}_{il}$), and two independent charge U(1)_l symmetries in both layers (generated by $N_l = \sum_i c_{i\uparrow}^{\dagger} c_{i\downarrow}$ for $l = 1, 2$). \mathbb{Z}_2^{F} indicates the fermion parity symmetry shared between SU(2) and U(1)₁ × U(1)₂. The U(1)₁ × U(1)₂ group may also be rewritten as U(1)₊ ×_{ℤ₂^F U(1)₋ with U(1)_± generated by $N_{\pm} = N_1 \pm N_2$, a more convenient notion for later discussions.}

Given these symmetries, for a generic non-integer filling fraction ν (i.e. 4ν electrons per unit cell), the system is subject to the Fermi surface anomaly [36–39, 57–66], and its ground state must either remain gapless (metallic) or become gapped at the price of developing spontaneous symmetry breaking (SSB) order or topological order. Mathematically, the classification of Fermi surface anomaly [66] for a given internal symmetry group $G \supset \mathbb{Z}_2^F$ is governed by the cobordism group [67–71] $\text{TP}_1(\text{Spin} \times_{\mathbb{Z}_2^F} G)$. By taking $G = G_{\text{general}}$ in Eq. (2), we arrive at the following classification

$$\text{TP}_1(\text{Spin} \times_{\mathbb{Z}_2^F} G_{\text{general}}) = \mathbb{Z} \times \mathbb{Z}, \quad (3)$$

signifying the presence of two perturbative local anomalies, each associated with one $U(1)$ symmetry. The Fermi surface anomaly is generally non-vanishing unless the filling fractions for both $U(1)$ symmetries are integers. This situation makes it impossible to trivially gap out Fermion excitations on the Fermi surface, thereby precluding the realization of a featureless insulating state.

III. ANALYSIS

A. SMG Insulator at Half-Filling

However, an exception occurs when the system is half-filled ($\nu = 1/2$), corresponding to zero chemical potential $\mu = 0$ in the lattice model Eq. (1) and an average of two electrons per unit cell. In this case, the lattice model possesses a larger internal symmetry

$$G_{\text{half-filled}} = \text{SU}(2) \times_{\mathbb{Z}_2^F} (\text{SU}(2)_1 \times \text{SU}(2)_2), \quad (4)$$

promoting both $U(1)_l$ ($l = 1, 2$) symmetries to $\text{SU}(2)_l$. The $\text{SU}(2)_l$ groups are generated by $\mathbf{K}_l = \sum_i \mathbf{K}_{il}$ with $\mathbf{K}_{il} := \frac{1}{2}(-)^i \tilde{c}_{il}^\dagger \boldsymbol{\sigma} \tilde{c}_{il}$, where $\tilde{c}_{il} = (c_{i\uparrow}, c_{i\downarrow})^\top$ is the Nambu spinor and $(-)^i$ denotes the stagger sign of momentum (π, π) on the square lattice.

Plugging the enlarged symmetry group $G_{\text{half-filled}}$ in Eq. (4) into the Fermi surface anomaly classification formula, we obtain

$$\text{TP}_1(\text{Spin} \times_{\mathbb{Z}_2^F} G_{\text{half-filled}}) = 0, \quad (5)$$

meaning that the Fermi surface anomaly is trivialized to no anomaly at half-filling. Since $G_{\text{general}} \subset G_{\text{half-filled}}$, this suggests a trivialization of the anomaly in a subgroup G_{general} by an injective pushforward to anomaly-free in a larger group $G_{\text{half-filled}}$ through an injective (one-to-one) homomorphism ι via $G_{\text{general}} \xrightarrow{\iota} G_{\text{half-filled}}$; somehow its novelty is *different* from the Symmetry Extension surjective pullback trivialization mechanism [72–75] which uses a pullback to trivialize an anomaly in a quotient group G_Q to anomaly-free in an extended total group \tilde{G} , under a surjective (onto) homomorphism $s: \tilde{G} \xrightarrow{s} G_Q$. Physically, the anomaly cancellation at half-filling is because

each unit cell with two electrons can realize the trivial (singlet) representation of all $\text{SU}(2)$ symmetries simultaneously. This enables the fermion system to be gapped into a symmetric product state, permitted by the LSM theorem.

However, the three $\text{SU}(2)$ symmetries are too restrictive, that they rule out all possible Fermi bilinear gapping terms, as enumerated in Tab. I. Therefore, symmetric gapping can only be driven by interaction effects intrinsically without any mean-field-level interpretation — a mechanism known as SMG [27]. The interlayer Heisenberg interaction in Eq. (1) is one such symmetric gapping interaction, as to be elaborated later. The resulting gapped state is called an SMG insulator — a featureless Mott insulator unique to bilayer lattice systems like nickelates, and it can not be realized in single-layer systems such as cuprates due to the Fermi surface anomaly (or the LSM anomaly).

TABLE I. Classification of all on-site fermion bilinear gapping terms (local order parameters) by symmetry representations, including: intralayer pairings $\Delta_{il} \simeq c_{il}^\dagger \sigma^2 c_{il}$ and density waves $(\Phi_{il}, \mathbf{\Phi}_{il}) \simeq (-)^i c_{il}^\dagger \sigma^\mu c_{il}$, interlayer pairings $(\Delta_i, \mathbf{\Delta}_i) \simeq c_{i1}^\dagger i \sigma^2 \sigma^\mu c_{i2}$ and excitons $(\Phi_i, \mathbf{\Phi}_i) \simeq (-)^i c_{i1}^\dagger \sigma^\mu c_{i2}$.

| | SU(2) | SU(2) ₁ | SU(2) ₂ | U(1) ₁ | U(1) ₂ | Bilinear order | Energy |
|---|-------|--------------------|--------------------|-------------------|--|----------------|--------|
| 1 | 3 | 1 | ±2 0 | 0 0 | $\Delta_{i1}^\dagger, \Delta_{i1}$ Φ_{i1} | 0 | |
| | | | | | | | 1 |
| | 2 | 2 | ±1 ±1 | ±1 ∓1 | $\Delta_i^\dagger, \Delta_i$ Φ_i^\dagger, Φ_i | −3J/4 | |
| 3 | 1 | 1 | 0 0 | 0 0 | $\Phi_{i1} + \Phi_{i2}$ $\Phi_{i1} - \Phi_{i2}$ | +J/2 −J/2 | |
| | | | | | | | 2 |

The phase diagram of the model Hamiltonian H in Eq. (1) at half-filling $\nu = 1/2$ has been examined by Ref. 34, with the key findings being:

- (i) In the larger J/t regime, H has a unique symmetric gapped ground state, smoothly deformable from the product state of interlayer spin-singlet state $\prod_i (c_{i1\uparrow}^\dagger c_{i2\downarrow}^\dagger - c_{i1\downarrow}^\dagger c_{i2\uparrow}^\dagger) |0\rangle_c$. This state preserves all lattice and internal $\text{SU}(2) \times_{\mathbb{Z}_2^F} (\text{SU}(2)_1 \times \text{SU}(2)_2)$ symmetries, and opens a gap (generating a fermion mass) on the Fermi surface, hence called the SMG insulator [32]. It has no SSB or topological order. Its existence is enabled by anomaly cancellation [65, 66] within the bilayer system.
- (ii) In the smaller J/t regime, due to Fermi surface instability at weak coupling, SSB order emerges in the system. Tab. I summarizes all possible local SSB orders. The last column lists the mean-field energy of condensing each order parameter, i.e., the Hubbard-Stratonovich decomposition coefficient of

the interlayer Heisenberg interaction J in each ordering channel. The leading SSB order (of the lowest energy $-3J/4$) appears either as an s -wave interlayer spin-singlet superconductivity (SC), described by $\langle \Delta_i \rangle \simeq \langle c_{i1}^\dagger i \sigma^2 c_{i2} \rangle \neq 0$, or as a (π, π) -momentum interlayer spin-singlet exciton condensation (EC), defined by $\langle \Phi_i \rangle \simeq (-)^i \langle c_{i1}^\dagger c_{i2} \rangle \neq 0$. The two SSB orders are degenerate in energy due to the $SU(2)_1 \times SU(2)_2$ symmetry at half-filling. Both orders fully gap the Fermi surface, while breaking either the total charge $U(1)_+$ symmetry (for the SC order) or the interlayer charge-difference $U(1)_-$ and lattice translation symmetries (for the EC order).

The SMG insulator can be considered a trivial insulator, achieved by restoring the broken $U(1)_\pm$ symmetry via disordering the $U(1)_\pm$ phase angle of the local order parameter, while still preserving the local Fermion gap. Upon (either electron or hole) doping away from the half-filling, the $SU(2)_1 \times SU(2)_2$ symmetry is broken explicitly, such that SC and EC are no longer energetically degenerated. The s -wave SC order is more favorable and becomes the unique leading SSB order, because of its perfect particle-hole Fermi surface nesting. Therefore, the high- T_c SC observed in $\text{La}_3\text{Ni}_2\text{O}_7$ could be interpreted as the SC phase that arises from hole doping SMG insulator from $\nu = 1/2$ to: (i) either $\nu = 1/4$ for $d_{x^2-y^2}$ electrons (ii) or $\nu = 1/2 - \delta$ (with a small δ) for d_{z^2} electrons. To differentiate the two possibilities and to understand the doping effect more quantitatively, we investigate the SC phase in the lattice model Eq. (1) from both the weak coupling (BCS) and strong coupling (BEC) perspectives in the following.

B. Weak Coupling Analysis

In the non-interacting limit ($J = 0$), the Hamiltonian H in Eq. (1) presents a free fermion band model, with a 4-fold (layer and spin) degenerated Fermi surface at generic filling. This free fermion state becomes unstable under the perturbative interaction J . In the weak coupling regime ($J/t \lesssim 1$), the mean-field energetic analysis in Tab. I suggests the leading instability occurs in the interlayer spin-singlet pairing channel, corresponding to the following Cooper pair creation operator

$$\Delta_i^\dagger = \frac{1}{\sqrt{2}}(c_{i1\uparrow}^\dagger c_{i2\downarrow}^\dagger - c_{i1\downarrow}^\dagger c_{i2\uparrow}^\dagger). \quad (6)$$

Given the decomposition $\mathbf{S}_{i1} \cdot \mathbf{S}_{i2} = -\frac{1}{2}(\Delta_i^\dagger \Delta_i + \Delta_i \Delta_i^\dagger) + \frac{1}{4}((n_{i1}-1)(n_{i2}-1)+1)$ (where $n_{il} := c_{il}^\dagger c_{il}$), we can formulate a Bardeen-Cooper-Schrieffer (BCS) mean-field theory assuming an s -wave order parameter $\langle \Delta_i \rangle = \Delta$,

$$H_{\text{BCS}}[\Delta] = \sum_{\mathbf{k}} \left(\sum_l c_{\mathbf{k}l}^\dagger (\epsilon_{\mathbf{k}} - \mu) c_{\mathbf{k}l} - J \left(\frac{1}{\sqrt{2}} \Delta c_{\mathbf{k}1}^\dagger i \sigma^2 c_{\mathbf{k}2}^\dagger + \text{h.c.} - |\Delta|^2 \right) \right), \quad (7)$$

where $\epsilon_{\mathbf{k}} = 2t(\cos k_x + \cos k_y)$ models the band dispersion. The optimal Δ emerges from minimizing the mean-field free energy $F_{\text{BCS}}[\Delta] = -\frac{1}{\beta} \ln \text{Tr} e^{-\beta H_{\text{BCS}}[\Delta]}$. Taking the saddle point equation $\delta F_{\text{BCS}}[\Delta]/\delta \Delta = 0$ at the $\Delta \rightarrow 0$ limit, we can compute the SC transition temperature T_c (setting $k_B = 1$) from

$$\frac{1}{J} = \int \frac{d^2 \mathbf{k}}{(2\pi)^2} \frac{1}{2\xi_{\mathbf{k}}} \tanh \frac{\xi_{\mathbf{k}}}{2T_c}, \quad (8)$$

and determine the fermion filling ν at T_c by $\nu = \frac{1}{2}(1 - \int \frac{d^2 \mathbf{k}}{(2\pi)^2} \tanh \frac{\xi_{\mathbf{k}}}{2T_c})$ given $\xi_{\mathbf{k}} := \epsilon_{\mathbf{k}} - \mu$. The result is shown in Fig. 3(a).

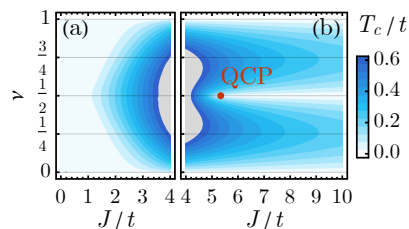


FIG. 3. The SC transition temperature T_c depending on the interaction strength J/t and the filling fraction ν , estimated by (a) the BCS mean-field theory for weak coupling, and (b) the BEC mean-field theory for strong coupling. The gray regions indicate areas where mean-field theories are about to fail.

In the simplest form, the BCS theory predicts that T_c should scale with the coupling strength J as $T_c \propto e^{-1/g_{\text{F}} J}$, where g_{F} denotes the Fermi surface density of state (DOS). The T_c vanishes either by $J = 0$ or by $g_{\text{F}} = 0$ (along $\nu = 0, 1$). The maximum T_c occurs around $\nu = 1/2$, due to the divergent DOS at the half-filling. These basic features are all manifest in Fig. 3(a).

C. Strong Coupling Analysis

We continue to consider the strong coupling mechanism, where SC emerges from doping the SMG insulator. Given that the SMG insulator already has preformed interlayer Cooper pairs in a Mott insulating state at half-filling (one Cooper pair per site), doping enables these Cooper pairs to gain mobility and condense into a superfluid (SF) state at low temperatures, manifesting as an SC state for electrons.

In the strong coupling regime ($J/t \gg 1$), we postulate the low-energy subspace to be the Hilbert space of Cooper pairs, denoted as $\mathcal{H}^\Delta = \bigotimes_i \mathcal{H}_i^\Delta$, where

$$\mathcal{H}_i^\Delta = \text{span}\{|0\rangle_c, \Delta_i^\dagger |0\rangle_c, (\Delta_i^\dagger)^2 |0\rangle_c\} \quad (9)$$

defines the on-site Hilbert space [76]. By reducing the model Hamiltonian H in Eq. (1) to the low-energy subspace \mathcal{H}^Δ up to the 2nd order perturbation in t/J , we

arrive at an effective Hamiltonian \tilde{H} for Cooper pairs

$$\tilde{H} = -\tilde{t} \sum_{\langle ij \rangle} (\Delta_i^\dagger \Delta_j + \text{h.c.}) - \sum_i (2\mu N_{i-} + \frac{3}{4} J N_{i+}). \quad (10)$$

where $\tilde{t} = 8t^2/3J$ is the effective hopping of Cooper pairs, and $N_{i\pm} := \Delta_i^\dagger \Delta_i \pm \Delta_i \Delta_i^\dagger$ are pair interaction (N_{i+}) and pair density (N_{i-}) operators. The Cooper pair chemical potential μ will be tuned to adjust the electron filling fraction ν effectively.

To proceed, we introduce the mean-field order parameter $\langle \Delta_i \rangle = \Delta$ to decouple the Hamiltonian \tilde{H} to each site, as

$$H_{\text{BEC}}[\Delta] = - \sum_i \left(4\tilde{t}(\Delta \Delta_i^\dagger + \text{h.c.} - |\Delta|^2) + 2\mu N_{i-} + \frac{3}{4} J N_{i+} \right). \quad (11)$$

The ground state energy $E_{\text{BEC}}[\Delta]$ of the mean-field Hamiltonian $H_{\text{BEC}}[\Delta]$ can be found by diagonalizing the many-body problem on each site independently (in a 3-dimensional on-site Hilbert space). The vacuum expectation value Δ can be obtained by solving the saddle point equation $\delta E_{\text{BEC}}[\Delta]/\delta \Delta = 0$ to minimize the ground state energy E_{BEC} . The solution of Δ determines the SF density $\rho_s = |\Delta|^2$ at zero-temperature ($T = 0$). Upon raising to a finite temperature ($T > 0$), the broken $U(1)_+$ charge conservation symmetry will be restored by thermal fluctuations. The transition temperature can be estimated from the Kosterlitz-Thouless transition [77] temperature $T_c = \pi \tilde{t} \rho_s = (8\pi t^2/3J)|\Delta|^2$. The result is shown in Fig. 3(b).

In the large J/t limit, the SC transition temperature T_c vanishes at $\nu = 0, 1/2, 1$, marking different Mott insulating states of Cooper pairs, with 0, 1, 2 Cooper pairs per unit cell, respectively. In terms of electrons, $\nu = 0, 1$ corresponds to band insulators, where T_c vanishes for all J/t values, owing to the absence of itinerant charge carriers. The insulating state at $\nu = 1/2$ is particularly noteworthy, which corresponds to the SMG insulator, a featureless Mott insulator only attainable in bilayer lattice systems for spin-1/2 fermions, as a result of anomaly cancellation.

The BEC mean-field analysis reveals a quantum critical point (QCP) at $J_c/t = 16/3 \approx 5.33$, where the SMG insulating phase ends, giving way to the SC phase. This QCP represents an SF-Mott transition for Cooper pairs and belongs to the (2+1)D XY universality class. Crossing this QCP (along $\nu = 1/2$ with an increase in J/t), the electron single-particle excitation gap persists, while the phase coherence of Cooper pairs in the SC phase gets destroyed in the SMG phase, restoring the broken $U(1)_+$ symmetry.

A key characteristic of the SMG insulator is that it is filling-enforced: since the necessary condition for the SMG to occur is anomaly cancellation, which takes place only at half-filling. As a result, if the SMG insulator is

doped away from half-filling, it cannot remain featureless. The BEC mean-field analysis reveals that a superconducting (SC) order is promptly established by either electron or hole doping from $\nu = 1/2$. The peak of T_c is reached around $\nu = 1/2 \pm 1/4$ fillings, where the mobility of the Cooper pairs is at its strongest. These attributes are demonstrated in Fig. 3(b).

D. BCS-BEC Crossover

The weak-coupling BCS and strong-coupling BEC analysis both identify the same s-wave interlayer spin-singlet SC state, implying the existence of a unified SC phase that crosses over between the BCS and BEC regimes. To qualitatively unify these two pictures, as presented in Fig. 3(a,b), into a single phase diagram, we employ a simple-minded smooth interpolation to estimate the SC transition temperature as:

$$T_c = \frac{T_{\text{BCS}} + T_{\text{BEC}}}{2} - T_0 \ln \left(2 \cosh \left(\frac{T_{\text{BCS}} - T_{\text{BEC}}}{2T_0} \right) \right). \quad (12)$$

Here, T_{BCS} and T_{BEC} represent the critical temperatures predicted by the BCS and BEC theories, respectively, and T_0 is a temperature scale governing the smoothness of the interpolation. When $T_0 = 0$, Eq. (12) reduces to $T_c = \min(T_{\text{BCS}}, T_{\text{BEC}})$. We choose $T_0 \simeq 0.067t$, which gives a reasonable interpolation as shown in Fig. 4. The phase diagram in Fig. 1(b) is also produced with this interpolation scheme. A more rigorous calculation of T_c could be performed using quantum Monte Carlo (QMC) or variational Monte Carlo (VMC) simulations, but we will leave them for future research.

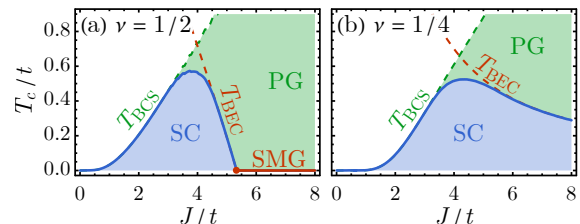


FIG. 4. SC transition temperature T_c estimated by a smooth interpolation between BCS and BEC theories, for (a) $\nu = 1/2$ and (b) $\nu = 1/4$ fillings, corresponding to two horizontal cuts in Fig. 1(b). On the BEC side, a pseudo-gap (PG) phase appears above T_c with incoherent preformed Cooper pairs fluctuating at low energy.

As the interaction strength J/t increases, the critical temperature T_c exhibits a behavior that first increases (in the BCS regime) and then decreases (in the BEC regime). The BCS-BEC crossover occurs between these two regimes, where T_c reaches its maximum value. The decline of T_c within the BEC regime is associated with the decreasing effective hopping $\tilde{t} = 8t^2/3J$ of Cooper pairs, which hinders the ability of Cooper pairs to establish phase coherence. At $\nu = 1/2$, as illustrated in

Fig. 4(a), the T_c drops to zero at the QCP $J_c/t = 16/3$, where the SMG insulator emerges. For other fillings, such as $\nu = 1/4$, the SMG phase is forbidden by the Fermi surface anomaly, so the SC phase theoretically extends to the $J/t \rightarrow \infty$ limit, as in Fig. 4(b).

T_{BCS} defines the temperature scale below which the interlayer Cooper pair forms. In the strong coupling regime, however, the Cooper pair will not establish the phase coherence and condense into the SF state, unless the temperature is lowered further below T_{BEC} . Thus, for large J/t , there exists an intermediate temperature range $T_{\text{BEC}} < T < T_{\text{BCS}}$, where the system resides in a pseudo-gap (PG) phase. The PG phase is characterized by locally fluctuating preformed Cooper pairs that lack long-range phase coherence. Itinerant electrons or holes scattering with these low-energy fluctuations can give rise to anomalous metallic behavior, such as resistivity that is linearly proportional to temperature, known as the strange metal behavior.

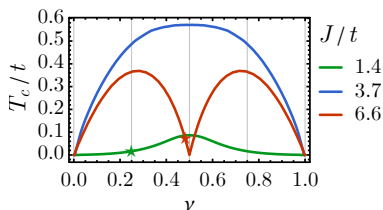


FIG. 5. Filling dependence of the SC transition temperature T_c at different values of J/t , corresponding to three vertical cuts in Fig. 1(b): green - $J/t = 1.4$ in the BCS regime, relevant to $d_{x^2-y^2}$ electrons; blue - $J/t = 3.7$ in the crossover regime, where T_c reaches global maximum; red - $J/t = 6.6$ in the BEC regime, relevant to d_{z^2} electrons.

At a fixed interaction strength J/t , the relationship between the critical temperature T_c and the electron filling fraction ν is illustrated in Fig. 5. In the weak-coupling BCS regime (such as $J/t = 1.4$), the maximal T_c is found at half-filling due to the divergent DOS at that point. In contrast, in the strong-coupling BEC regime (such as $J/t = 6.6$), the emergence of the SMG insulator at half-filling forces T_c to vanish at $\nu = 1/2$ and pushes the maximum T_c position towards $\nu = 1/4$ (or $3/4$) as $J/t \rightarrow \infty$, corresponding to 50% hole (or electron) doping away from the SMG insulator. Clearly, doping the SMG insulator is an effective approach to induce high-temperature superconductivity, as only a small amount of doping could lead to a substantial increase in T_c , as shown in Fig. 5 (red curve). However, the highest T_c is actually reached in the BCS-BEC crossover region within this model around $J/t = 3.7$, although experimentally attaining this region in real materials might be challenging.

IV. DISCUSSIONS

A. Application to Pressurized $\text{La}_3\text{Ni}_2\text{O}_7$

We explore the high- T_c SC behavior of the pressurized $\text{La}_3\text{Ni}_2\text{O}_7$ based on the mean-field understanding of the bilayer square lattice model Eq. (1), as summarized in the phase diagram Fig. 1(b). Tab. II enumerates our estimates for the model parameters relevant to the Ni $d_{x^2-y^2}$ and d_{z^2} electrons.

TABLE II. Parameter estimation and theory predicted T_c for Ni $d_{x^2-y^2}$ and d_{z^2} electrons. Meaning of symbols: ν - filling fraction, t - hopping parameter, J - interlayer Heisenberg coupling strength, T_c - estimated SC transition temperature.

| | $d_{x^2-y^2}$ electron | d_{z^2} electron |
|------------------|--------------------------------|-------------------------|
| ν | 1/4 | 1/2 \rightarrow 0.483 |
| t | 0.48 eV | \sim 0.1 eV |
| J | \sim 0.66 eV | |
| J/t | 1.4 | 6.6 |
| T_c/t (theory) | 0.014 | 0 \rightarrow 0.067 |
| T_c (theory) | 79 K | 0 \rightarrow 78 K |
| SC order | s-wave interlayer spin-singlet | |
| Mechanism | BCS | BEC |

According to these estimates,

- (i) The itinerant $d_{x^2-y^2}$ electrons are likely located at $(J/t, \nu) = (1.4, 1/4)$ in the SC phase on the BCS side, marked as the green star in Fig. 1(b), where the BCS mean-field theory predicts a SC transition temperature of the order $T_c \simeq 79$ K.
- (ii) In contrast, d_{z^2} electrons are natively positioned at $(J/t, \nu) = (6.6, 1/2)$, right in the SMG insulating phase, which does not contribute to SC (i.e., $T_c = 0$). However, given the sensitivity of the SMG insulator to the filling fraction, an infinitesimal amount of doping can immediately drive the SMG insulator into a superconductor.

We demonstrate that hole doping this SMG insulator by as small as 3.4% to $(J/t, \nu) = (6.6, 0.483)$ can place d_{z^2} electrons in the SC phase on the BEC side, denoted by the red star in Fig. 1(b), with an SC transition temperature drastically increased to $T_c \simeq 78$ K, predicted by the BEC mean-field theory. DFT calculations [1, 7] indicate that after applying pressure, the d_{z^2} band top may surpass the Fermi level, forming a smaller hole pocket, which lends support for a small amount of hole doping.

Therefore, both $d_{x^2-y^2}$ and d_{z^2} electrons can achieve high- T_c SC states within the bilayer square lattice minimal model. The SC order involves s-wave interlayer spin-singlet pairing, driven by the interlayer antiferromagnetic Heisenberg interaction of electrons. In the phase diagram, their SC states belong to the same SC phase

that emerges from doping the SMG insulator (this notion might be more appropriate for d_{z^2} electrons on the BEC side). It is worth noting that the observed strange metal behavior in experiments [1, 2, 4] can be interpreted through the interaction between the two degrees of freedom: the d_{z^2} electrons first form preformed incoherent Cooper pairs, which then scatter with the itinerant electrons/holes in the system, leading to the strange metal behavior. The itinerant freedom in this context may originate from either $d_{x^2-y^2}$ or d_{z^2} orbitals.

Judging solely from the SC transition temperature, it is challenging to determine whether the SC in $\text{La}_3\text{Ni}_2\text{O}_7$ system originates from d_{z^2} or $d_{x^2-y^2}$ electrons, as both can result in an SC transition temperature close to 80K within a reasonable parameter range. Furthermore, the strange metal behavior neither suffice to distinguish between the two cases. This uncertainty arises because it is unclear which temperature is higher between the two: the BEC temperature of the preformed pairs of d_{z^2} electrons or the pairing temperature of the $d_{x^2-y^2}$ electrons. Therefore, additional experimental evidence should be considered.

On the one hand, the phenomenon of T_c decreasing with increasing pressure [1, 3] favors the d_{z^2} as the dominant degree of freedom responsible for SC. In fact, as the pressure increases, the distance between the NiO_2 layers decreases, and the interlayer superexchange interaction J strengthens. If SC is in the BEC regime, the T_c will indeed decrease with the increase in J . This pressure effect is harder to understand if SC is in the BCS regime.

On the other hand, there are also compelling arguments in favor of the $d_{x^2-y^2}$ as the dominant role for SC. Firstly, some studies [20] have shown that Hund's rule interaction has a strong renormalization effect on the d_{z^2} band, leading to a significant reduction in its bandwidth and a remarkable decrease in its superconducting transition temperature. In contrast, $d_{x^2-y^2}$ has better itinerancy, making it a better candidate for SC to emerge. Secondly, for the SC resulting from doping SMG insulator, one of the most prominent features is that the optimal T_c is achieved around quarter filling. This optimal filling nicely coincides with the filling of the $d_{x^2-y^2}$ orbitals, speaking for its potential of realizing high- T_c SC. Finally, although the J/t value of the $d_{x^2-y^2}$ orbital listed in Table II is only 1.4, considering the no-double-occupancy constraint brought by the strong Hubbard interaction (see below), the effective t would be renormalized by a Gutzwiller factor of about $\delta = 0.5$, under which the value of J/t doubles, which can significantly enhance the T_c .

In summary, there might be simultaneous superconductivity in both d_{z^2} and $d_{x^2-y^2}$ orbitals in the $\text{La}_3\text{Ni}_2\text{O}_7$ system. We propose that a key piece of evidence to distinguish between them might lie in studying the dependence of T_c on doping. If the SC is dominated by $d_{x^2-y^2}$ electrons under the BCS mechanism, its T_c will increase with *electron* doping. If the SC is dominated by d_{z^2} electrons under the BEC mechanism, its T_c will increase with

hole doping. These two diametrically opposite behaviors can provide a clear distinction in determining the electronic orbital origin of SC in pressurized $\text{La}_3\text{Ni}_2\text{O}_7$ systems. Moreover, the feature of the phase transition from SC to the normal state is different between the BEC and BCS pictures. On the BEC side, the phase transition is driven by kinetic-energy gain. Consequently, the spectrum weight in the optical conductivity will shift toward the low-frequency side. Such spectrum weight shifts in the optical conductivity will not be detected in the BCS transition.

B. Hubbard Interaction and Strong Correlation Effects

In our minimal model, we ignored the on-site Hubbard interaction among d -orbital electrons. Including the Hubbard interaction would amplify the electron correlation effects, manifesting as intralayer antiferromagnetic Heisenberg interaction through the superexchange mechanism. This promotes antiferromagnetic (AFM) fluctuations within each layer, potentially leading to long-range AFM order or intralayer d -wave SC, reminiscent of the physics in cuprates. Generally, these SSB-ordered phases could compete with the interlayer SC, leading to alternative phases [21, 54–56].

However, analyses [21, 22] indicated that, for both d_{z^2} and $d_{x^2-y^2}$ electrons, the intralayer AFM coupling is weaker than the interlayer coupling. Within this parameter regime, intralayer AFM correlations actually facilitate the interlayer pairing for superconductivity. Studies [78, 79] on a two-leg ladder t - J model with both intra- and inter-chain Heisenberg interactions reveal that, upon hole doping, the system develops SC quasi-long-range order with inter-chain spin-singlet pairing. The mobility of a single hole on a short-range AFM-correlated chain is hindered due to the phase string effect [80–82], which refers to a \mathbb{Z}_2 Berry phase accumulated when the hole exchanges with specific background spins. This destructive interference effect reduces hole mobility and acts against superconductivity. However, because of the \mathbb{Z}_2 nature of the phase string effect, it is canceled if two holes across the chains are paired and move together. This results in the promotion of inter-chain pairing by the short-range AFM correlation along the chain. Such kinetic-energy-driven pairing mechanism has been studied in the bilayer square lattice very recently [83], indicating an enhanced interlayer spin-singlet pairing from the phase string effect in the presence of Hubbard interaction.

V. SUMMARY

We investigate the emergent superconductivity from doping an SMG insulator in a bilayer square lattice model, which encompasses intralayer hopping t and interlayer antiferromagnetic Heisenberg interaction J of spin-

1/2 fermions. This minimal model is proposed to capture the essential physics of the Ni d -orbital electrons in the nickelate superconductor $\text{La}_3\text{Ni}_2\text{O}_7$.

We highlight the manifestation of an SMG insulator in the strong coupling $J/t \gg 1$ regime at half-filling — a featureless Mott insulator facilitated by the cancellation of LSM anomaly in bilayer lattice systems. Our analysis reveals that doping the SMG insulator can lead to superconductivity, with an s -wave interlayer spin-singlet pairing. The SC phase exhibits BCS-BEC crossover by tuning the J/t ratio. Our main result is the mean-field phase diagram presented in Fig. 1(b), providing a unified understanding of the SC originated from both Ni $3d_{z^2}$ and $3d_{x^2-y^2}$ orbitals.

On the strong-coupling BEC side, the SC transition temperature T_c reduces with the interlayer interaction strength J , which provides insights into the decreasing T_c with pressure in the $\text{La}_3\text{Ni}_2\text{O}_7$ superconductor. Above T_c , a pseudo-gap phase emerges, in which strange metal behavior is expected, consistent with experimental observation. Furthermore, our findings suggest that both Ni $3d_{z^2}$ and $3d_{x^2-y^2}$ orbitals can exhibit SC in pressurized $\text{La}_3\text{Ni}_2\text{O}_7$. We propose future experimental studies of the doping dependence of the critical temperature

T_c or the spectral weight transfer in optical conductivity, which could likely provide experimental tests to determine which electron orbital mainly contributes to the superconducting formation.

ACKNOWLEDGMENTS

We acknowledge insightful discussions with Meng Wang, Yi-Fan Jiang, Zi-Xiang Li, Zheyang Wan, Zheng-Yu Weng, Hao-Kai Zhang, Hui Zhai, and Yang Qi. M.L., Z.Y.Z., and Y.Z.Y. acknowledge the hospitality of Institute for Advanced Study at Tsinghua University, where part of the research was performed. J.W. thanks the hospitality of IBM Thomas J. Watson Research Center and Guanyu Zhu. D.C.L., W.H., and Y.Z.Y. are supported by the National Science Foundation (NSF) Grant No. DMR-2238360. F.Y. is supported by the National Natural Science Foundation of China under the Grant No. 12074031, No. 12234016, No. 11674025. J.W. is supported by the Center for Mathematical Sciences and Applications at Harvard University and the NSF Grant DMS-1607871. We acknowledge the OpenAI GPT4 model for providing language suggestions in writing this paper.

-
- [1] H. Sun, M. Huo, X. Hu, J. Li, Y. Han, L. Tang, Z. Mao, P. Yang, B. Wang, J. Cheng, D.-X. Yao, G.-M. Zhang, and M. Wang, Signatures of superconductivity near 80 k in a nickelate under high pressure, *Nature* [10.1038/s41586-023-06408-7](https://doi.org/10.1038/s41586-023-06408-7) (2023), [arXiv:2305.09586](https://arxiv.org/abs/2305.09586) [cond-mat.supr-con].
- [2] Z. Liu, M. Huo, J. Li, Q. Li, Y. Liu, Y. Dai, X. Zhou, J. Hao, Y. Lu, M. Wang, and H.-H. Wen, Electronic correlations and energy gap in the bilayer nickelate $\text{La}_3\text{Ni}_2\text{O}_7$, [arXiv e-prints](https://arxiv.org/abs/2307.02950), [arXiv:2307.02950](https://arxiv.org/abs/2307.02950) (2023), [arXiv:2307.02950](https://arxiv.org/abs/2307.02950) [cond-mat.supr-con].
- [3] J. Hou, P. T. Yang, Z. Y. Liu, J. Y. Li, P. F. Shan, L. Ma, G. Wang, N. N. Wang, H. Z. Guo, J. P. Sun, Y. Uwatoko, M. Wang, G. M. Zhang, B. S. Wang, and J. G. Cheng, Emergence of high-temperature superconducting phase in the pressurized $\text{La}_3\text{Ni}_2\text{O}_7$ crystals, [arXiv e-prints](https://arxiv.org/abs/2307.09865), [arXiv:2307.09865](https://arxiv.org/abs/2307.09865) (2023), [arXiv:2307.09865](https://arxiv.org/abs/2307.09865) [cond-mat.supr-con].
- [4] Y. Zhang, D. Su, Y. Huang, H. Sun, M. Huo, Z. Shan, K. Ye, Z. Yang, R. Li, M. Smidman, M. Wang, L. Jiao, and H. Yuan, High-temperature superconductivity with zero-resistance and strange metal behavior in $\text{La}_3\text{Ni}_2\text{O}_7$, [arXiv e-prints](https://arxiv.org/abs/2307.14819), [arXiv:2307.14819](https://arxiv.org/abs/2307.14819) (2023), [arXiv:2307.14819](https://arxiv.org/abs/2307.14819) [cond-mat.supr-con].
- [5] P. A. Lee, N. Nagaosa, and X.-G. Wen, Doping a Mott insulator: Physics of high-temperature superconductivity, *Reviews of Modern Physics* **78**, 17 (2006).
- [6] B. Keimer, S. A. Kivelson, M. R. Norman, S. Uchida, and J. Zaanen, From quantum matter to high-temperature superconductivity in copper oxides, *Nature (London)* **518**, 179 (2015).
- [7] Z. Luo, X. Hu, M. Wang, W. Wú, and D.-X. Yao, Bilayer two-orbital model of $\text{La}_3\text{Ni}_2\text{O}_7$ under pressure, [arXiv e-prints](https://arxiv.org/abs/2305.15564), [arXiv:2305.15564](https://arxiv.org/abs/2305.15564) (2023), [arXiv:2305.15564](https://arxiv.org/abs/2305.15564) [cond-mat.supr-con].
- [8] Y. Zhang, L.-F. Lin, A. Moreo, and E. Dagotto, Electronic structure, orbital-selective behavior, and magnetic tendencies in the bilayer nickelate superconductor $\text{La}_3\text{Ni}_2\text{O}_7$ under pressure, [arXiv e-prints](https://arxiv.org/abs/2306.03231), [arXiv:2306.03231](https://arxiv.org/abs/2306.03231) (2023), [arXiv:2306.03231](https://arxiv.org/abs/2306.03231) [cond-mat.supr-con].
- [9] V. Christiansson, F. Petocchi, and P. Werner, Correlated electronic structure of $\text{La}_3\text{Ni}_2\text{O}_7$ under pressure, [arXiv e-prints](https://arxiv.org/abs/2306.07931), [arXiv:2306.07931](https://arxiv.org/abs/2306.07931) (2023), [arXiv:2306.07931](https://arxiv.org/abs/2306.07931) [cond-mat.str-el].
- [10] D. A. Shilenko and I. V. Leonov, Correlated electronic structure, orbital-selective behavior, and magnetic correlations in double-layer $\text{La}_3\text{Ni}_2\text{O}_7$ under pressure, [arXiv e-prints](https://arxiv.org/abs/2306.14841), [arXiv:2306.14841](https://arxiv.org/abs/2306.14841) (2023), [arXiv:2306.14841](https://arxiv.org/abs/2306.14841) [cond-mat.str-el].
- [11] H. Sakakibara, N. Kitamine, M. Ochi, and K. Kuroki, Possible high T_c superconductivity in $\text{La}_3\text{Ni}_2\text{O}_7$ under high pressure through manifestation of a nearly-half-filled bilayer Hubbard model, [arXiv e-prints](https://arxiv.org/abs/2306.06039), [arXiv:2306.06039](https://arxiv.org/abs/2306.06039) (2023), [arXiv:2306.06039](https://arxiv.org/abs/2306.06039) [cond-mat.supr-con].
- [12] Q.-G. Yang, D. Wang, and Q.-H. Wang, Possible S_{\pm} -wave superconductivity in $\text{La}_3\text{Ni}_2\text{O}_7$, [arXiv e-prints](https://arxiv.org/abs/2306.03706), [arXiv:2306.03706](https://arxiv.org/abs/2306.03706) (2023), [arXiv:2306.03706](https://arxiv.org/abs/2306.03706) [cond-mat.supr-con].
- [13] Y. Gu, C. Le, Z. Yang, X. Wu, and J. Hu, Effective model and pairing tendency in bilayer Ni-based superconductor $\text{La}_3\text{Ni}_2\text{O}_7$, [arXiv e-prints](https://arxiv.org/abs/2306.07275), [arXiv:2306.07275](https://arxiv.org/abs/2306.07275) (2023), [arXiv:2306.07275](https://arxiv.org/abs/2306.07275) [cond-mat.supr-con].
- [14] Y.-B. Liu, J.-W. Mei, F. Ye, W.-Q. Chen, and F. Yang,

- The s^{\pm} -Wave Pairing and the Destructive Role of Apical-Oxygen Deficiencies in $\text{La}_3\text{Ni}_2\text{O}_7$ Under Pressure, [arXiv e-prints](#), [arXiv:2307.10144](#) (2023), [arXiv:2307.10144](#) [[cond-mat.supr-con](#)].
- [15] Y. Zhang, L.-F. Lin, A. Moreo, T. A. Maier, and E. Dagotto, Structural phase transition, s_{\pm} -wave pairing and magnetic stripe order in the bilayered nickelate superconductor $\text{La}_3\text{Ni}_2\text{O}_7$ under pressure, [arXiv e-prints](#), [arXiv:2307.15276](#) (2023), [arXiv:2307.15276](#) [[cond-mat.supr-con](#)].
- [16] Y. Zhang, L.-F. Lin, A. Moreo, T. A. Maier, and E. Dagotto, Trends of electronic structures and s_{\pm} -wave pairing for the rare-earth series in bilayer nickelate superconductor $R_3\text{Ni}_2\text{O}_7$, [arXiv e-prints](#), [arXiv:2308.07386](#) (2023), [arXiv:2308.07386](#) [[cond-mat.supr-con](#)].
- [17] F. Lechermann, J. Gondolf, S. Bötzel, and I. M. Eremin, Electronic correlations and superconducting instability in $\text{La}_3\text{Ni}_2\text{O}_7$ under high pressure, [arXiv e-prints](#), [arXiv:2306.05121](#) (2023), [arXiv:2306.05121](#) [[cond-mat.str-el](#)].
- [18] Y. Shen, M. Qin, and G.-M. Zhang, Effective bilayer model Hamiltonian and density-matrix renormalization group study for the high- T_c superconductivity in $\text{La}_3\text{Ni}_2\text{O}_7$ under high pressure, [arXiv e-prints](#), [arXiv:2306.07837](#) (2023), [arXiv:2306.07837](#) [[cond-mat.str-el](#)].
- [19] W. Wú, Z. Luo, D.-X. Yao, and M. Wang, Charge Transfer and Zhang-Rice Singlet Bands in the Nickelate Superconductor $\text{La}_3\text{Ni}_2\text{O}_7$ under Pressure, [arXiv e-prints](#), [arXiv:2307.05662](#) (2023), [arXiv:2307.05662](#) [[cond-mat.str-el](#)].
- [20] Y. Cao and Y.-F. Yang, Flat bands promoted by Hund's rule coupling in the candidate double-layer high-temperature superconductor $\text{La}_3\text{Ni}_2\text{O}_7$, [arXiv e-prints](#), [arXiv:2307.06806](#) (2023), [arXiv:2307.06806](#) [[cond-mat.supr-con](#)].
- [21] C. Lu, Z. Pan, F. Yang, and C. Wu, Interlayer Coupling Driven High-Temperature Superconductivity in $\text{La}_3\text{Ni}_2\text{O}_7$ Under Pressure, [arXiv e-prints](#), [arXiv:2307.14965](#) (2023), [arXiv:2307.14965](#) [[cond-mat.supr-con](#)].
- [22] H. Oh and Y.-H. Zhang, Type II t-J model and shared antiferromagnetic spin coupling from Hund's rule in superconducting $\text{La}_3\text{Ni}_2\text{O}_7$, [arXiv e-prints](#), [arXiv:2307.15706](#) (2023), [arXiv:2307.15706](#) [[cond-mat.str-el](#)].
- [23] X.-Z. Qu, D.-W. Qu, J. Chen, C. Wu, F. Yang, W. Li, and G. Su, Bilayer t - J - J_{\perp} Model and Magnetically Mediated Pairing in the Pressurized Nickelate $\text{La}_3\text{Ni}_2\text{O}_7$, [arXiv e-prints](#), [arXiv:2307.16873](#) (2023), [arXiv:2307.16873](#) [[cond-mat.str-el](#)].
- [24] Y.-F. Yang, G.-M. Zhang, and F.-C. Zhang, Minimal effective model and possible high- T_c mechanism for superconductivity of $\text{La}_3\text{Ni}_2\text{O}_7$ under high pressure, [arXiv e-prints](#), [arXiv:2308.01176](#) (2023), [arXiv:2308.01176](#) [[cond-mat.supr-con](#)].
- [25] Z. Liao, L. Chen, G. Duan, Y. Wang, C. Liu, R. Yu, and Q. Si, Electron correlations and superconductivity in $\text{La}_3\text{Ni}_2\text{O}_7$ under pressure tuning, [arXiv e-prints](#), [arXiv:2307.16697](#) (2023), [arXiv:2307.16697](#) [[cond-mat.supr-con](#)].
- [26] K. Jiang, Z. Wang, and F.-C. Zhang, High Temperature Superconductivity in $\text{La}_3\text{Ni}_2\text{O}_7$, [arXiv e-prints](#), [arXiv:2308.06771](#) (2023), [arXiv:2308.06771](#) [[cond-mat.supr-con](#)].
- [27] J. Wang and Y.-Z. You, Symmetric Mass Generation, *Symmetry* **14**, 1475 (2022), [arXiv:2204.14271](#) [[cond-mat.str-el](#)].
- [28] K. Slagle, Y.-Z. You, and C. Xu, Exotic quantum phase transitions of strongly interacting topological insulators, *Phys. Rev. B* **91**, 115121 (2015), [arXiv:1409.7401](#) [[cond-mat.str-el](#)].
- [29] Y.-Y. He, H.-Q. Wu, Y.-Z. You, C. Xu, Z. Y. Meng, and Z.-Y. Lu, Quantum critical point of Dirac fermion mass generation without spontaneous symmetry breaking, *Phys. Rev. B* **94**, 241111 (2016), [arXiv:1603.08376](#) [[cond-mat.str-el](#)].
- [30] Y.-Z. You, Y.-C. He, C. Xu, and A. Vishwanath, Symmetric Fermion Mass Generation as Deconfined Quantum Criticality, *Physical Review X* **8**, 011026 (2018), [arXiv:1705.09313](#) [[cond-mat.str-el](#)].
- [31] Y.-Z. You, Y.-C. He, A. Vishwanath, and C. Xu, From bosonic topological transition to symmetric fermion mass generation, *Phys. Rev. B* **97**, 125112 (2018), [arXiv:1711.00863](#) [[cond-mat.str-el](#)].
- [32] D.-C. Lu, M. Zeng, J. Wang, and Y.-Z. You, Fermi surface symmetric mass generation, *Phys. Rev. B* **107**, 195133 (2023), [arXiv:2210.16304](#) [[cond-mat.str-el](#)].
- [33] W. Hou and Y.-Z. You, Variational Monte Carlo Study of Symmetric Mass Generation in a Bilayer Honeycomb Lattice Model, [arXiv e-prints](#), [arXiv:2212.13364](#) (2022), [arXiv:2212.13364](#) [[cond-mat.str-el](#)].
- [34] D.-C. Lu, M. Zeng, and Y.-Z. You, Green's Function Zeros in Fermi Surface Symmetric Mass Generation, [arXiv e-prints](#), [arXiv:2307.12223](#) (2023), [arXiv:2307.12223](#) [[cond-mat.str-el](#)].
- [35] E. Lieb, T. Schultz, and D. Mattis, Two soluble models of an antiferromagnetic chain, *Annals of Physics* **16**, 407 (1961).
- [36] M. Oshikawa, Topological Approach to Luttinger's Theorem and the Fermi Surface of a Kondo Lattice, *Phys. Rev. Lett.* **84**, 3370 (2000), [arXiv:cond-mat/0002392](#) [[cond-mat.str-el](#)].
- [37] M. Cheng, M. Zaletel, M. Barkeshli, A. Vishwanath, and P. Bonderson, Translational Symmetry and Microscopic Constraints on Symmetry-Enriched Topological Phases: A View from the Surface, *Physical Review X* **6**, 041068 (2016), [arXiv:1511.02263](#) [[cond-mat.str-el](#)].
- [38] G. Y. Cho, C.-T. Hsieh, and S. Ryu, Anomaly manifestation of Lieb-Schultz-Mattis theorem and topological phases, *Phys. Rev. B* **96**, 195105 (2017), [arXiv:1705.03892](#) [[cond-mat.str-el](#)].
- [39] N. Bultinck and M. Cheng, Filling constraints on fermionic topological order in zero magnetic field, *Phys. Rev. B* **98**, 161119 (2018), [arXiv:1808.00324](#) [[cond-mat.str-el](#)].
- [40] M. B. Hastings, Sufficient conditions for topological order in insulators, *EPL (Europhysics Letters)* **70**, 824 (2005), [arXiv:cond-mat/0411094](#) [[cond-mat.str-el](#)].
- [41] D. P. Arovas, E. Berg, S. A. Kivelson, and S. Raghu, The Hubbard Model, *Annual Review of Condensed Matter Physics* **13**, 239 (2022), [arXiv:2103.12097](#) [[cond-mat.str-el](#)].
- [42] I. Bloch, J. Dalibard, and W. Zwerger, Many-body physics with ultracold gases, *Reviews of Modern Physics* **80**, 885 (2008), [arXiv:0704.3011](#) [[cond-mat.other](#)].
- [43] W. Zwerger, *The BCS-BEC crossover and the unitary Fermi gas*, Vol. 836 (Springer Science & Business Media, 2011).

- [44] H. A. Gersch and G. C. Knollman, Quantum Cell Model for Bosons, *Physical Review* **129**, 959 (1963).
- [45] M. Ma, B. I. Halperin, and P. A. Lee, Strongly disordered superfluids: Quantum fluctuations and critical behavior, *Phys. Rev. B* **34**, 3136 (1986).
- [46] M. P. A. Fisher, P. B. Weichman, G. Grinstein, and D. S. Fisher, Boson localization and the superfluid-insulator transition, *Phys. Rev. B* **40**, 546 (1989).
- [47] J. Bardeen, L. N. Cooper, and J. R. Schrieffer, Microscopic theory of superconductivity, *Phys. Rev.* **106**, 162 (1957).
- [48] J. Bardeen, L. N. Cooper, and J. R. Schrieffer, Theory of superconductivity, *Phys. Rev.* **108**, 1175 (1957).
- [49] I. Kimchi, S. A. Parameswaran, A. M. Turner, F. Wang, and A. Vishwanath, Featureless and nonfractionalized Mott insulators on the honeycomb lattice at 1/2 site filling, *Proceedings of the National Academy of Science* **110**, 16378 (2013), arXiv:1207.0498 [cond-mat.str-el].
- [50] H. Zhai, F. Wang, and D.-H. Lee, Antiferromagnetically driven electronic correlations in iron pnictides and cuprates, *Phys. Rev. B* **80**, 064517 (2009), arXiv:0905.1711 [cond-mat.supr-con].
- [51] Y.-H. Zhang and S. Sachdev, From the pseudogap metal to the Fermi liquid using ancilla qubits, *Physical Review Research* **2**, 023172 (2020), arXiv:2001.09159 [cond-mat.str-el].
- [52] Y.-H. Zhang and S. Sachdev, Deconfined criticality and ghost Fermi surfaces at the onset of antiferromagnetism in a metal, *Phys. Rev. B* **102**, 155124 (2020), arXiv:2006.01140 [cond-mat.str-el].
- [53] A. Nikolaenko, M. Tikhanovskaya, S. Sachdev, and Y.-H. Zhang, Small to large Fermi surface transition in a single-band model using randomly coupled ancillas, *Phys. Rev. B* **103**, 235138 (2021), arXiv:2103.05009 [cond-mat.str-el].
- [54] A. Bohrdt, L. Homeier, C. Reinmoser, E. Demler, and F. Grusdt, Exploration of doped quantum magnets with ultracold atoms, *Annals of Physics* **435**, 168651 (2021), arXiv:2107.08043 [cond-mat.quant-gas].
- [55] A. Bohrdt, L. Homeier, I. Bloch, E. Demler, and F. Grusdt, Strong pairing in mixed-dimensional bilayer antiferromagnetic Mott insulators, *Nature Physics* **18**, 651 (2022), arXiv:2108.04118 [cond-mat.str-el].
- [56] S. Hirthe, T. Chalopin, D. Bourgund, P. Bojović, A. Bohrdt, E. Demler, F. Grusdt, I. Bloch, and T. A. Hilker, Magnetically mediated hole pairing in fermionic ladders of ultracold atoms, *Nature (London)* **613**, 463 (2023), arXiv:2203.10027 [cond-mat.quant-gas].
- [57] A. Paramekanti and A. Vishwanath, Extending Luttinger's theorem to \mathbb{Z}_2 fractionalized phases of matter, *Phys. Rev. B* **70**, 245118 (2004), arXiv:cond-mat/0406619 [cond-mat.str-el].
- [58] X.-Y. Song, Y.-C. He, A. Vishwanath, and C. Wang, Electric polarization as a nonquantized topological response and boundary Luttinger theorem, arXiv e-prints, arXiv:1909.08637 (2019), arXiv:1909.08637 [cond-mat.mes-hall].
- [59] X.-G. Wen, Low-energy effective field theories of fermion liquids and the mixed $U(1) \times \mathbb{R}^d$ anomaly, *Phys. Rev. B* **103**, 165126 (2021), arXiv:2101.08772 [cond-mat.str-el].
- [60] D. V. Else, R. Thorngren, and T. Senthil, Non-Fermi Liquids as Ersatz Fermi Liquids: General Constraints on Compressible Metals, *Physical Review X* **11**, 021005 (2021), arXiv:2007.07896 [cond-mat.str-el].
- [61] D. V. Else and T. Senthil, Strange Metals as Ersatz Fermi Liquids, *Phys. Rev. Lett.* **127**, 086601 (2021), arXiv:2010.10523 [cond-mat.str-el].
- [62] R. Ma and C. Wang, Emergent anomaly of Fermi surfaces: a simple derivation from Weyl fermions, arXiv e-prints, arXiv:2110.09492 (2021), arXiv:2110.09492 [cond-mat.str-el].
- [63] C. Wang, A. Hickey, X. Ying, and A. A. Burkov, Emergent anomalies and generalized Luttinger theorems in metals and semimetals, *Phys. Rev. B* **104**, 235113 (2021), arXiv:2110.10692 [cond-mat.str-el].
- [64] Z. Darius Shi, H. Goldman, D. V. Else, and T. Senthil, Gifts from anomalies: Exact results for Landau phase transitions in metals, *SciPost Phys.* **13**, 102 (2022), arXiv:2204.07585 [cond-mat.str-el].
- [65] M. Cheng and N. Seiberg, Lieb-Schultz-Mattis, Luttinger, and 't Hooft - anomaly matching in lattice systems, arXiv e-prints, arXiv:2211.12543 (2022), arXiv:2211.12543 [cond-mat.str-el].
- [66] D.-C. Lu, J. Wang, and Y.-Z. You, Definition and Classification of Fermi Surface Anomalies, arXiv e-prints, arXiv:2302.12731 (2023), arXiv:2302.12731 [cond-mat.str-el].
- [67] A. Kapustin, R. Thorngren, A. Turzillo, and Z. Wang, Fermionic symmetry protected topological phases and cobordisms, *Journal of High Energy Physics* **2015**, 52 (2015), arXiv:1406.7329 [cond-mat.str-el].
- [68] D. S. Freed and M. J. Hopkins, Reflection positivity and invertible topological phases, arXiv e-prints, arXiv:1604.06527 (2016), arXiv:1604.06527 [hep-th].
- [69] M. Guo, P. Putrov, and J. Wang, Time reversal, $SU(N)$ Yang-Mills and cobordisms: Interacting topological superconductors/insulators and quantum spin liquids in $3 + 1$ D, *Annals of Physics* **394**, 244 (2018), arXiv:1711.11587 [cond-mat.str-el].
- [70] Z. Wan and J. Wang, Higher Anomalies, Higher Symmetries, and Cobordisms I: Classification of Higher-Symmetry-Protected Topological States and Their Boundary Fermionic/Bosonic Anomalies via a Generalized Cobordism Theory, arXiv e-prints, arXiv:1812.11967 (2018), arXiv:1812.11967 [hep-th].
- [71] M. Guo, K. Ohmori, P. Putrov, Z. Wan, and J. Wang, Fermionic Finite-Group Gauge Theories and Interacting Symmetric/Crystalline Orders via Cobordisms, *Communications in Mathematical Physics* **376**, 1073 (2020), arXiv:1812.11959 [hep-th].
- [72] J. Wang, X.-G. Wen, and E. Witten, Symmetric Gapped Interfaces of SPT and SET States: Systematic Constructions, *Phys. Rev. X* **8**, 031048 (2018), arXiv:1705.06728 [cond-mat.str-el].
- [73] J. Wang, K. Ohmori, P. Putrov, Y. Zheng, Z. Wan, M. Guo, H. Lin, P. Gao, and S.-T. Yau, Tunneling Topological Vacua via Extended Operators: (Spin-)TQFT Spectra and Boundary Deconfinement in Various Dimensions, *PTEP* **2018**, 053A01 (2018), arXiv:1801.05416 [cond-mat.str-el].
- [74] A. Prakash, J. Wang, and T.-C. Wei, Unwinding Short-Range Entanglement, *Phys. Rev. B* **98**, 125108 (2018), arXiv:1804.11236 [quant-ph].
- [75] A. Prakash and J. Wang, Unwinding fermionic symmetry-protected topological phases: Supersymmetry extension, *Phys. Rev. B* **103**, 085130 (2021), arXiv:2011.13921 [cond-mat.str-el].
- [76] Note that each site (with two layers) can host at most

- two Cooper pairs.
- [77] J. M. Kosterlitz and D. J. Thouless, Ordering, metastability and phase transitions in two-dimensional systems, *Journal of Physics C: Solid State Physics* **6**, 1181 (1973).
 - [78] S. Chen, Z. Zhu, and Z.-Y. Weng, Two-hole ground state wavefunction: Non-BCS pairing in a t -J two-leg ladder, *Phys. Rev. B* **98**, 245138 (2018), [arXiv:1808.06173 \[cond-mat.str-el\]](#).
 - [79] H.-K. Zhang, R.-Y. Sun, and Z.-Y. Weng, Pair density wave characterized by a hidden string order parameter, [arXiv e-prints](#) , [arXiv:2212.06170 \(2022\)](#), [arXiv:2212.06170 \[cond-mat.str-el\]](#).
 - [80] D. N. Sheng, Y. C. Chen, and Z. Y. Weng, Phase String Effect in a Doped Antiferromagnet, *Phys. Rev. Lett.* **77**, 5102 (1996).
 - [81] Z. Y. Weng, D. N. Sheng, Y. C. Chen, and C. S. Ting, Phase string effect in the t-J model: General theory, *Phys. Rev. B* **55**, 3894 (1997), [arXiv:cond-mat/9612040 \[cond-mat.str-el\]](#).
 - [82] Z.-Y. Weng, Superconducting ground state of a doped Mott insulator, *New Journal of Physics* **13**, 103039 (2011), [arXiv:1105.3027 \[cond-mat.supr-con\]](#).
 - [83] J.-X. Zhang, H.-K. Zhang, Y.-Z. You, and Z.-Y. Weng, Strong Pairing Originated from an Emergent \mathbb{Z}_2 Berry Phase in $\text{La}_3\text{Ni}_2\text{O}_7$, [arXiv e-prints](#) , [arXiv:2309.05726 \(2023\)](#), [arXiv:2309.05726 \[cond-mat.str-el\]](#).